IOP Publishing | Institute of Physics and Engineering in Medicine Physics in Medicine & Biology

Phys. Med. Biol. **60** (2015) 1641–1654 doi:10.1088/0031-9155/60/4/1641

Towards a quantitative, measurement-based estimate of the uncertainty in photon mass attenuation coefficients at radiation therapy energies

E S M Ali[1,3], B Spencer[1,4], M R McEwen[2] and D W O Rogers[1]

[1] Department of Physics, Carleton University, Ottawa, Canada
[2] Ionizing Radiation Standards, National Research Council, Ottawa, Canada

E-mail: elali@toh.on.ca and drogers@physics.carleton.ca

Received 14 July 2014, revised 12 November 2014
Accepted for publication 8 December 2014
Published 26 January 2015

Abstract

In this study, a quantitative estimate is derived for the uncertainty in the XCOM photon mass attenuation coefficients in the energy range of interest to external beam radiation therapy—i.e. 100 keV (orthovoltage) to 25 MeV—using direct comparisons of experimental data against Monte Carlo models and theoretical XCOM data. Two independent datasets are used. The first dataset is from our recent transmission measurements and the corresponding EGSnrc calculations (Ali *et al* 2012 *Med. Phys.* **39** 5990–6003) for 10–30 MV photon beams from the research linac at the National Research Council Canada. The attenuators are graphite and lead, with a total of 140 data points and an experimental uncertainty of ~0.5% ($k = 1$). An optimum energy-independent cross section scaling factor that minimizes the discrepancies between measurements and calculations is used to deduce cross section uncertainty. The second dataset is from the aggregate of cross section measurements in the literature for graphite and lead (49 experiments, 288 data points). The dataset is compared to the sum of the XCOM data plus the IAEA photonuclear data. Again, an optimum energy-independent cross section scaling factor is used to deduce the cross section uncertainty. Using the average result from the two datasets, the energy-independent cross section uncertainty estimate is 0.5% (68% confidence) and 0.7% (95% confidence). The potential for energy-dependent errors is discussed. Photon cross section uncertainty is shown to be smaller than the current qualitative 'envelope of uncertainty' of the order of 1–2%, as given by Hubbell (1999 *Phys. Med. Biol* **44** R1–22).

[3] Current affiliation: Department of Medical Physics, The Ottawa Hospital Cancer Centre, Ottawa, Canada
[4] Current affiliation: TIMC-IMAG Laboratory, Domaine de la Merci, 38706 La Tronche Cedex, France

Keywords: photon cross section uncertainty, cross section measurements, XCOM, EGSnrc, transmission

(Some figures may appear in colour only in the online journal)

1. Introduction

Photon mass attenuation coefficients, μ/ρ, are fundamental data that are used directly or indirectly in all photon dosimetric calculations (the coefficients for mass energy transfer, μ_{tr}/ρ, and mass energy absorption, μ_{en}/ρ, are also based on μ/ρ). A better knowledge of the uncertainty in μ/ρ allows for a more accurate estimate of the overall uncertainty in the dosimetric quantities of interest.

One of the most widely used μ/ρ datasets is the NIST XCOM database (Berger *et al* 2010), which is based on Hubbell (1982) and Hubbell and Seltzer (1995). XCOM does not include photonuclear cross sections, therefore all the uncertainty estimates below are made after the photonuclear component is added. Hubbell (1982) estimates the uncertainty in μ/ρ to be of the order of 5% below 5 keV, 2% up to 20 MeV (with photonuclear cross sections added), and 1% or better for light elements where incoherent scattering dominates (200 keV to 5 MeV). More recently, Hubbell (1999) notes that 'it has been difficult to establish an envelope of uncertainty as desired by workers in radiation dosimetry reference standards'. He suggests an 'envelope of uncertainty ... of the order of 1–2%' for 'the photon energy range of most interest in medical and biology applications, 5 keV to a few MeV'. Hubbell's envelope of uncertainty is determined by judging from the estimates of Cullen *et al* (1997) for the uncertainty in the photoelectric cross sections. While Hubbell (1999) assumes a 68% confidence bound for the uncertainty estimates by Cullen *et al* (1997) (see table 1 in Hubbell (1999)), no explicit confidence bounds are given by Hubbell (1999) for his envelope of uncertainty of 1–2% . In light of the uncertainty estimates in his earlier publication (Hubbell 1982), the 2% end of the envelope of uncertainty in Hubbell (1999) is more likely for the lower end of the quoted energy range, given the larger contribution of the photoelectric cross sections with their attendant uncertainties. The lack of more precise cross section uncertainty estimates with explicit confidence bounds is partially because different theoretical models for cross sections are limited in different ways, which makes it difficult to use the differences among models to establish the desired precise uncertainty. Somewhat equivalently, the evolution of measured and calculated cross section data versus time (as illustrated in table 2 of Hubbell (1999)) is also difficult to use for quantitative uncertainty estimates.

In recent years, the increase in the computing power and in the sophistication of Monte Carlo codes has led to the reduction of many statistical and systematic uncertainties. Consequently, the uncertainty in the underlying photon cross sections has become a more significant contributor to the overall uncertainty, and hence the need for more accurate and precise cross section uncertainty estimates has increased. Examples include Monte Carlo calculations for beam quality conversion factors (Muir and Rogers 2010, Wulff *et al* 2010), air kerma standards (Andreo *et al* 2012), unfolding photon spectra of clinical linacs (Ali and Rogers 2012, Ali *et al* 2012b), attenuation calculations (Walters *et al* 1997), and transmission analysis (Ali *et al* 2012a) where the uncertainty in μ/ρ is shown to be the ultimate limiting factor of the calculation accuracy.

The aim of this study is to derive an estimate of the uncertainty in photon mass attenuation coefficients that is more quantitative than the current estimate, has explicit confidence bounds, and is extracted from direct comparisons of experimental data against their respective Monte

Carlo or theoretical models. Two independent datasets are used, one of which is a new dataset that has not been previously used for cross section uncertainty estimates. The energy range in this study is the range of interest to external beam radiation therapy—namely from the lower end of orthovoltage energies (100 keV) to 25 MeV (although some data points in one of the two datasets used in the analysis extends to 40 MeV). The cross section dataset evaluated in this study is the XCOM database plus the IAEA evaluated photonuclear data (Varlamov *et al* 1999, IAEA 2000). This combination of cross section data (henceforth called 'XCOM + IAEA') is one of the more accurate cross section datasets available. The analysis is done for graphite and lead so as to span a wide range of atomic numbers. Using the results for both elements, a material-independent energy-independent uncertainty in μ/ρ is extracted. The additional uncertainties to arrive at μ_{tr}/ρ and μ_{en}/ρ are beyond the scope of this study. Similar to any uncertainty analysis work, the methods presented below require assumptions and are thus approximate. However, compared with the current estimates, the authors believe that this study represents a step forward towards a more quantitative estimate of cross section uncertainty.

2. Methods

In what follows, the terms statistical/systematic describe the *nature* of different errors, while the terms Type A/B describe the *method of evaluation* of the uncertainty due to a certain type of error, according to The ISO Guide on Uncertainty in Measurement (Bentley 2003).

2.1. First dataset: recent transmission measurements

The first dataset (Ali *et al* 2012a) is our recent transmission measurements and the respective EGSnrc (Kawrakow 2000, Kawrakow *et al* 2011) calculations. The experimental transmission data, T_{exp}, are for seven photon beams from 10 to 30 MV, produced from the research linac at the National Research Council Canada using different bremsstrahlung targets and no flattening filters. The MV/bremsstrahlung target combinations are: 10/Al, 15/Be, 15/Al, 15/Pb, 20/Al, 20/Pb and 30/Al. The attenuators are graphite and lead, and the detector is an Exradin A19 Farmer chamber with different buildup caps (tungsten alloy and polymethylmethacrylate). The total number of data points is 140 (70 per attenuator material). From a detailed uncertainty budget (table 2 in Ali *et al* (2012a)), the final uncertainty on T_{exp} is found to change from 0.3% to 0.6% as the transmission signal changes from 100% to ~1.7%. This includes the contribution from the uncertainties in the incident electron beam parameters (mean energy, energy spread, focal spot size and shape, and beam angular divergence). In particular, the uncertainty in the electron mean energy is a major contributor to the overall uncertainty for graphite but not for lead because of the difference in the energy dependence of μ/ρ for the two materials. For the 10 MV beam (the lowest stable energy on that linac), the range of uncertainty on T_{exp} is 0.5% to 0.9%, which is larger than the range for the other beams because of a combination of beam instability issues and the larger effect of the uncertainty in the mean incident electron energy for lower MV beams.

The corresponding EGSnrc-calculated data, T_{EGSnrc}, have a combined statistical and systematic uncertainty of ~0.3% (table 3 in Ali *et al* (2012a)), not including photon cross section uncertainty. The two new features that have recently been added in EGSnrc (Ali *et al* 2014) are used in the simulations. The first feature is modelling photonuclear attenuation (without modelling secondary particles), which affects T_{EGSnrc} by up to 5.6% . The second feature is using the exact XCOM data as input to the simulations (before this feature was added, the option to use XCOM in EGSnrc led to differences of 1% relative to the web XCOM data, largely because EGSnrc still used its internal incoherent scattering

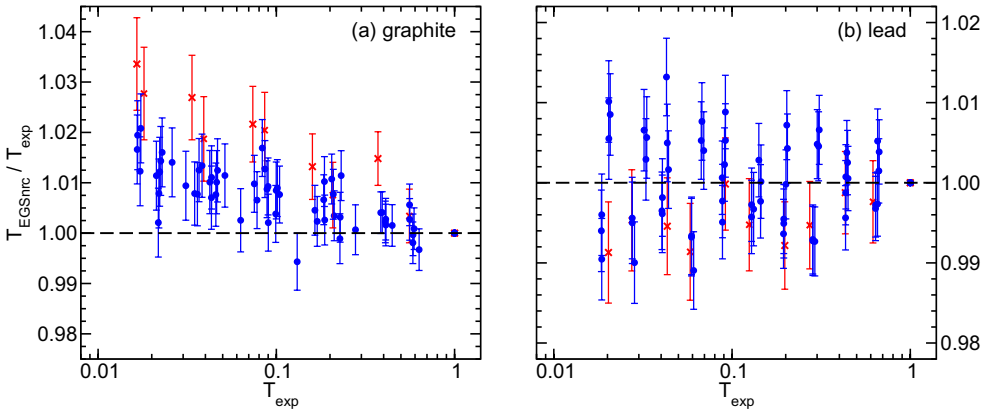

Figure 1. Ratios of the EGSnrc-calculated transmission data, T_{EGSnrc}, to experimental transmission signals, T_{exp}, for graphite attenuators (panel (*a*)) and for lead attenuators (panel (*b*)). The data in each panel are for 10–30 MV beams produced on the research linac of the National Research Council Canada using different bremsstrahlung targets (beryllium, aluminum and lead) and with the transmission data acquired using an Exradin A19 Farmer chamber with different buildup caps (tungsten alloy and polymethylmethacrylate). The 10 MV data are marked as × . The uncertainty bars (k = 1) include the experimental and Monte Carlo uncertainties. The uncertainty from the input photon cross sections is not included. The data in the figure is a condensed version of the results in Ali *et al* (2012a).

cross sections—see Ali *et al* (2014)). Figure 1 shows a condensed version of the level of agreement between T_{EGSnrc} and T_{exp}, as relevant to this study. The discrepancies are mostly within 2% for graphite attenuators (within 3.4% for 10 MV) and mostly within 1% for lead attenuators.

The transmission dataset is particularly useful for this study for four reasons. (1) The dataset has not been previously used for cross section uncertainty estimates. (2) The transmission data (particularly the smallest signals), are very sensitive to small cross section differences—e.g. changes in cross sections by 1% and 2% lead to changes in the smallest calculated transmission by 4% and 9%, respectively. (3) The incident electron parameters for the research linac used in the measurements are independently known (MacPherson and Ross 1998, Ross *et al* 2008). When these electron parameters are used in the Monte Carlo model, the model remains independent of the transmission (or similar, e.g. depth-dose) measurements. This eliminates circular arguments when using the comparison between measurements and calculations to extract photon cross section uncertainty. (4) Extensive Type A/B analysis has gone into studying the influence quantities in both the transmission measurements and their respective EGSnrc simulations, which minimizes potential systematic errors and leads to a small overall uncertainty, and to a small uncertainty on the uncertainty. This, in turn, makes it possible to attribute the discrepancy between calculations and measurements beyond the uncertainty bars to cross section errors.

2.2. Second dataset: cross section measurements in the literature

The second dataset is from the NIST bibliography compiled by Hubbell (www.nist.gov/pml/data/photon_cs/index.cfm), which contains a list of the publications that have experimental

measurements of photon cross sections in the literature up to the year 1995. For our study, the publications with μ/ρ values for graphite and lead are compiled and analyzed. The photon sources typically used for the measurements include radioactive sources, synchrotron radiation, nuclear reactions that produce gamma rays (e.g. neutron capture), and bremsstrahlung beams. The commonly used detectors are NaI(Tl), Ge(Li) and HPGe for direct spectroscopy, as well as Si(Li) detectors, ion chambers, and magnetic Compton spectrometers. Common sources of uncertainty include counting statistics, the contribution of small-angle scatter (coherent or incoherent), background effects, detector photopeak drifts, detection efficiency, energy calibration of the spectrometers, pulse pileup, detector deadtime corrections, exact energy of the radiation source, decay of the daughter nuclei in the source, energy variations in the bremsstrahlung beams when used as a source, inexact mass thicknesses of the attenuators, the effect of impurities in the attenuators, misalignment issues, and other setup uncertainties. The reported uncertainties in μ/ρ are typically $\sim$1%, but can be as small as 0.1% or as large as 5%.

The following set of qualifying criteria are applied to the available publications for graphite and lead. The experiment is published in or after 1950. It contains data in the energy range from 100 keV to 40 MeV. The publication seems to reasonably acknowledge and/or address the sources of systematic uncertainties. The reported uncertainty in μ/ρ is $\leqslant$2% . The reported μ/ρ values are within 4% of the current XCOM + IAEA data. The last criterion assumes that it is reasonable to consider our current knowledge of photon cross sections in the energy range of this study to be better than 4%, and it is put in place to ensure that an experiment with μ/ρ values that are very different from the average does not strongly drive the analysis, particularly if the corresponding reported uncertainty is unrealistically small. Based on these criteria, the total number of experiments included is 21 for graphite and 28 for lead. The number of data points is 183 for graphite and 105 for lead, with a total of 288 data points. The measured dataset is compared directly to the XCOM + IAEA data to estimate the cross section uncertainty.

2.3. Method of analysis

A generic description of the method of analysis is presented first, followed by the application of the method to the case of photon cross sections. When a model is compared against experimental measurements, the discrepancy (beyond the experimental uncertainty) can be used in a Type B analysis to estimate the systematic error in the model. Consider the tractable case where the systematic error in the model can be reasonably described by a single scaling factor. This systematic error can be determined by scaling the model with different values, α, and choosing the value, $\alpha_{\min}$, that minimizes the goodness-of-fit statistic χ_r^2, defined as

$$\chi_r^2 = \frac{1}{\nu}\sum_{i=1}^{N}\frac{\left(Y_{i,\mathrm{model}}(\alpha) - Y_{i,\mathrm{exp}}\right)^2}{s_{i,\mathrm{exp}}^2}, \tag{1}$$

where $Y_{i,\mathrm{exp}}$ is the ith experimental value, $Y_{i,\mathrm{model}}(\alpha)$ is the corresponding value calculated when the model is scaled by α, $s_{i,exp}$ is the estimated standard uncertainty on $Y_{i,\mathrm{exp}}$, N is the number of data points, ν is the number of degrees of freedom ($\nu = N - 1$ for the case of a single scaling factor), and χ_r^2 is the reduced χ^2 for ν degrees of freedom. This exercise is illustrated in figure 2. For the case where the model contains no errors, $\alpha_{\min}$ would be unity, and if the experimental uncertainties, $s_{i,\mathrm{exp}}$, have been properly assessed, then the value of χ_r^2 that

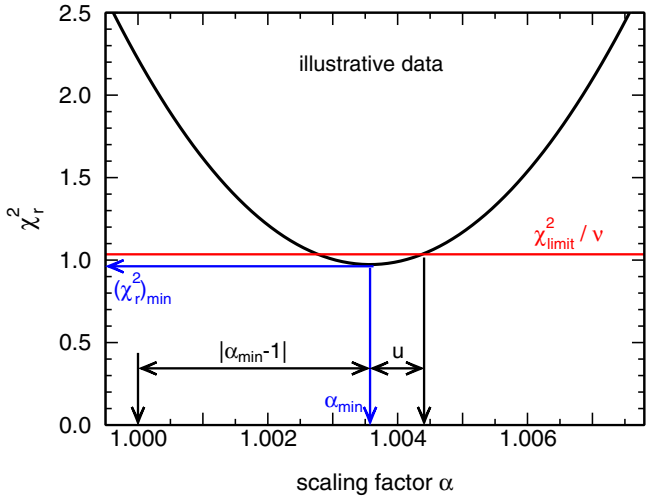

Figure 2. Illustration of the variation of the reduced χ^2 (defined in equation (1)) against the scaling factor of a model. Note that $\left(\chi_r^2\right)_{\min}$ is close to unity—see text for details.

corresponds to $\alpha_{\min}$ (denoted $\left(\chi_r^2\right)_{\min}$) would be close to unity. For the case where the model contains errors, the absolute deviation of $\alpha_{\min}$ from unity, i.e. $|\alpha_{\min} - 1|$ (expressed in per cent throughout this study), can be taken as a surrogate for the error in the model provided that $\left(\chi_r^2\right)_{\min}$ is not much larger than unity. Requiring $\left(\chi_r^2\right)_{\min}$ to not be much larger than unity is to ensure that the error in the model can be sufficiently described by a single scaling factor.

The value of $\alpha_{\min}$ determined using this method has uncertainty associated with it because of the presence of experimental uncertainties ($s_{i,exp}$ in equation (1)). Therefore the *uncertainty* (rather than the *error*) in the model can be described using a combination of $|\alpha_{\min} - 1|$ and its uncertainty, u (in per cent). The value of u can be determined using different approaches. One rigorous approach is the graphical method (Rogers 1975), described as follows. Define χ^2_{limit} as the limit value on χ^2 at a given confidence level, e.g. 68% . Dividing by the number of degrees of freedom, the limit value on χ_r^2 is $\chi^2_{\text{limit}} / \nu$. The absolute difference between the value of $\alpha_{\min}$ and the value of α that corresponds to $\chi^2_{\text{limit}} / \nu$ gives the value of u, as illustrated in figure 2. To determine χ^2_{limit} mentioned above, distinction between two cases needs to be made. In the first case, if a quantity is normally distributed and the actual uncertainty on its experimentally-measured values is known, then $\chi^2_{\text{limit}} = \chi^2_{\min} + N^2_\lambda$, where N_λ is the normal distribution at the λ% level (for λ = 68%, N_λ = 1). In the second case, if the knowledge of the experimental uncertainty is (or is assumed to be) only relative (i.e. the uncertainty is known up to a scaling factor), then $\chi^2_{\text{limit}} = \chi^2_{\min}\ [1 + F_\lambda(1, \nu) / \nu]$, where $F_\lambda(1, \nu)$ is the statistical F distribution with 1 and ν degrees of freedom for a given confidence level, λ (Rogers 1975). The difference in χ^2_{limit} calculated using the two methods is relatively small when the number of degrees of freedom is large. In our study, χ^2_{limit} is calculated both ways and the larger of the two values is taken. In addition to the graphical method, other Type B approaches can be used to determine u for situations such as data inconsistencies and/or large $\left(\chi_r^2\right)_{\min}$ values. Both the graphical method and other Type B approaches are used to determine u in this study.

When $\alpha_{\min}$ is close to unity, a conservative estimate of the uncertainty in the model (at a given confidence level) is to assume that it corresponds to *the maximal difference from unity*,

which can be determined as follows. Assuming that $\alpha_{\min}$ follows a normal distribution, then there is a 68% probability that $\alpha_{\min}$ falls in the interval $[\alpha_{\min} - u, \alpha_{\min} + u]$. Regardless of whether or not this interval encompasses unity, the furthest deviation from unity cannot be more than $|\alpha_{\min} - 1| + u$. Therefore there is *at least* a 68% probability that the uncertainty in the model is no larger than $(|\alpha_{\min} - 1| + u)\%$. Similarly, there is *at least* a 95% probability that the uncertainty in the model is no larger than $(|\alpha_{\min} - 1| + 2\,u)\%$. Note that the estimate of the 95% bound is not simply twice that for the 68% bound.

Now, the methods described above are applied to the case of photon cross sections as follows. As a first order estimate, cross section errors are assumed to be energy independent and can be described by a single scaling factor, which effectively assumes that the *functional shape* of the XCOM + IAEA data is a close representation of the true cross sections. The assumption of energy-independent errors is obviously crude since cross sections may have systematic errors versus energy as the relative contribution of different interaction processes changes with energy. For a given material, the optimum cross section scaling factor, $\alpha_{\min}$, is determined by minimizing the sum of the squares of the differences between the 'measurements' and the 'model', according to equation (1). For the first dataset (i.e. the transmission data), the measurements are the experimental transmission signals, and the model is the EGSnrc-calculated transmission data, with XCOM + IAEA data used as input to the simulations. In this case, what is sought is the $\alpha_{\min}$ value that achieves the best fit between the measured and calculated transmission data when $\alpha \times$ (XCOM + IAEA) data are used in EGSnrc. For the second dataset (i.e. the literature cross section data), the measurements are the experimental cross section data in the literature, and the model is XCOM + IAEA data (XCOM data are based on a collection of theoretical models). In this case, what is sought is the $\alpha_{\min}$ value that achieves the best fit between the measured cross section data in the literature and $\alpha \times$ (XCOM + IAEA). Once $\alpha_{\min}$ and u are determined, the 68% and 95% estimates of the cross section uncertainty are then $(|\alpha_{\min} - 1| + u)\%$ and $(|\alpha_{\min} - 1| + 2\,u)\%$, respectively.

2.4. Analysis of the recent transmission dataset

When applying the methods above to the transmission dataset, equation (1) is modified to include the estimated standard uncertainty in the Monte Carlo calculation, $s_{i,\mathrm{MC}}$, which includes statistical uncertainty and the uncertainty components from the detector energy response modelling, the Fano test, and the variation of the quantity W/e with energy (table 3 in Ali *et al* (2012a)), but it does not include photon cross section uncertainty. The modified equation is

$$\chi_r^2 = \frac{1}{\nu} \sum_{i=1}^{N} \frac{\left(Y_{i,\mathrm{model}}(\alpha) - Y_{i,\mathrm{exp}}\right)^2}{s_{i,\mathrm{exp}}^2 + s_{i,\mathrm{MC}}^2}\,. \tag{2}$$

The goal is to determine the $\alpha_{\min}$ value that minimizes the differences in figure 1 when $\alpha \times$ (XCOM + IAEA) data are used in EGSnrc. It would be computationally very intensive to systematically scale the attenuator cross sections by very small fractions of a per cent, and for each scaling factor repeat the large number of EGSnrc calculations for all the data points in figure 1 to statistical uncertainty smaller than the effect of the cross section changes on transmission (>100 h on a single CPU per data point per scaling factor). As an alternative, the following approach is used. Transmission data can be calculated deterministically using the following equation.

$$T(x_i) = \frac{\int_{E_l}^{E_m} R(E)\ \psi(E)\ \exp\left[-(\mu/\rho)(E)\ x_i\right]\ \mathrm{d}E}{\int_{E_l}^{E_m} R(E)\ \psi(E)\ \mathrm{d}E}, \tag{3}$$

where T is the transmission signal, x_i is the ith attenuator mass thickness, E is the photon energy, E_l and E_m are the lowest and maximum photon energies, respectively, $\psi(E)$ is the differential incident photon energy fluence, $R(E)$ is the detector energy response at E per unit $\psi(E)$, and $(\mu/\rho)(E)$ is the mass attenuation coefficient for the attenuator material at E. EGSnrc is used to pre-calculate $\psi(E)$ for the MV beams used, and to pre-calculate $R(E)$ for monoenergetic photon beams from a point source in the same experimental setup as the actual beams. To validate the use of equation (3), transmission values for different attenuator mass thicknesses are calculated with and without scaling of the cross sections of the attenuator materials, once using equation (3) and once using EGSnrc. The *ratios* of the transmission with to without cross section scaling calculated using equation (3) agree with the EGSnrc ratios to within the statistical precision of the EGSnrc calculations, which is <0.1% . Therefore for the rest of the analysis, equation (3) is used to calculate the transmission ratios that correspond to the cross section changes, and these ratios are used as *corrections* to the transmission data that are fully calculated only once using EGSnrc without cross section scaling. There are two assumptions in using equation (3) for the corrections instead of a full Monte Carlo calculation. (1) Non-ideal effects such as forward scatter that still reaches the detector are assumed to not change with small cross section changes. (2) The small cross section changes are applied to the attenuator material only, and not to the components of the linac or the detector that may contain the same material, and the assumption is that the potential minor changes in $\psi(E)$ and $R(E)$ that are ignored have a negligible effect on the calculated corrections. Both assumptions are found to be correct to within 0.1% for the small cross section changes made in this study. Given that the calculations using equation (3) are instantaneous, the resolution of the cross section scaling increments is chosen to be very small (0.01%). For each scaling factor, χ_r^2 is calculated for all MV beams together, and also for each beam separately to shed some light onto possible energy-dependent errors.

2.5. Analysis of the literature dataset

The goal is to determine the $\alpha_{\min}$ value that minimizes the differences between the experimental cross section data from the literature and $\alpha \times$ (XCOM + IAEA). The XCOM data that are used in the analysis are queried online with a very fine energy grid (2000 points) to minimize interpolation artifacts. The resolution of the cross section scaling increments is 0.05% . For each scaling factor, χ_r^2 is calculated for graphite and lead separately. The ratios of the experimental cross section data to the XCOM + IAEA data, after the optimum scaling is applied, are studied versus energy to explore possible energy-dependent errors.

3. Results and discussion

3.1. Estimate using the recent transmission dataset

For the transmission dataset, the variation of the reduced χ^2 versus the scaling factor is shown in figure 3. The smoothness of the curves is because of the use of the deterministic (rather than Monte Carlo) calculations for a very fine resolution of the scaling factor.

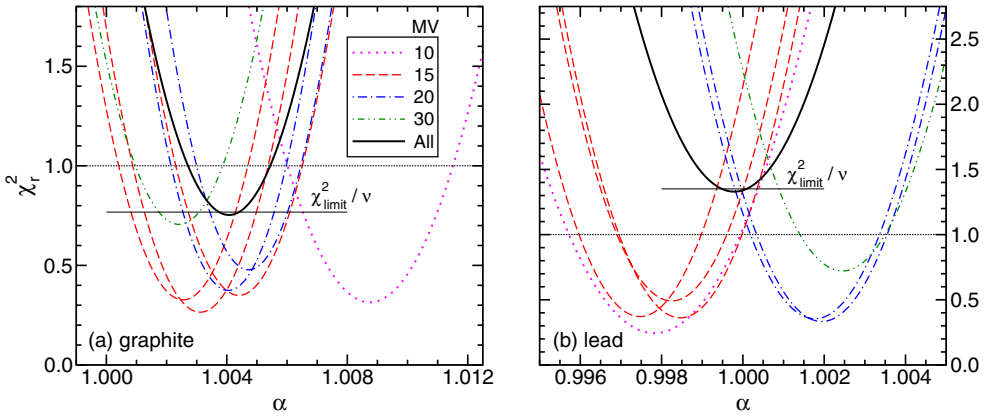

Figure 3. For the transmission dataset, variation of the reduced χ^2 when the input photon cross sections to EGSnrc (i.e. XCOM + IAEA data) are uniformly scaled by α. Panel (*a*) is for the graphite attenuators and panel (*b*) is for the lead attenuators. χ^2_{limit}/ν is the limit value on χ^2_r at the 68% confidence level for ν degrees of freedom (69 for all data combined). For a given MV beam and a given attenuator material, the different curves are for the same incident electron beam with different bremsstrahlung targets: Al for 10 MV (one dotted line); Be, Al and Pb for 15 MV (three dashed lines); Al and Pb for 20 MV(two dash-dot lines); and Al for 30 MV (one dash-double-dot line).

For graphite using the combined data from all the MV beams (70 data points and 69 degrees of freedom), $\alpha_{min} - 1$ is +0.41% and $\left(\chi^2_r\right)_{min}$ is 0.8. When the graphite cross section data are scaled by +0.41%, the ratios in figure 1(*a*) become scattered mostly within 0.5% around unity (which is comparable to the experimental uncertainties), except for the 10 MV data which become mostly 1% larger than unity. The value of u determined using the graphical method is 0.05%. Therefore the corresponding 68% estimate of graphite cross section uncertainty is $|+0.41| + 0.05 = 0.46\%$, and the 95% estimate is $|+0.41| + 2 \times 0.05 = 0.51\%$. When each MV beam is optimized individually (9 degrees of freedom per beam), $\alpha_{min} - 1$ varies from +0.25% to +0.88% (a spread of 0.63%), as shown in figure 3(*a*). The corresponding individual values of $\left(\chi^2_r\right)_{min}$ per beam are always smaller than unity (~ 0.4 on average), and are also smaller than the $\left(\chi^2_r\right)_{min}$ value of all the beams combined. When the individual $\alpha_{min} - 1$ values are plotted against the fluence-weighted mean energy of each MV beam (not shown), the results do not show any trend with energy. In figure 3(*a*), the range of the spread of the $\alpha_{min} - 1$ values of the individual beams (i.e. 0.63%) is substantially larger than the value of u determined using the graphical method (i.e. 0.05%). The spread is centred around the α_{min} value of all the beams combined, and (by definition) the spread contains 100% of the α_{min} values (i.e. it contains more than 95% of the values). Therefore half the 0.63% spread can be taken as the 95% interval (i.e. $2u$) and thus $u = 0.16\%$. Based on this, more representative 68% and 95% estimates of the graphite cross section uncertainty are $|+0.41| + 0.16 = 0.57\%$ and $|+0.41| + 2 \times 0.16 = 0.73\%$, respectively.

For lead with all the beam data combined, $\alpha_{min} - 1$ is –0.02% and $\left(\chi^2_r\right)_{min}$ is 1.3. When the lead cross section data are scaled by –0.02%, the ratios in figure 1(*b*) remain basically unchanged because the scaling is very small. The value of u from the graphical method is 0.04%, and the corresponding 68% and 95% estimates of lead cross section uncertainty are 0.06% and 0.10%, respectively. For the individual beams, $\alpha_{min} - 1$ varies from –0.25% to +0.25% (a spread of 0.50%), as shown in figure 3(*b*). Although the overall $\left(\chi^2_r\right)_{min}$ is

somewhat larger than unity (i.e. 1.3), its value for the individual beams is always much smaller than unity (~ 0.4 on average). Unlike graphite data, plotting the individual $\alpha_{\min} - 1$ values versus the fluence-weighted mean energy (not shown) indicates a positive correlation (the linear correlation coefficient is 0.78) in which the scaling factor varies by ~0.5% over the mean energy range from 1.5 MeV (for 10 MV) to 5.3 MeV (for 30 MV). When the XCOM + IAEA data are scaled by this linear model for the variation of the cross section error with energy, $\left(\chi_r^2\right)_{\min}$ does not get closer to unity, but rather worsens from 1.3 to 2.3. There are two possible reasons for this. (1) Representing each spectrum with the single metric of mean energy is an over-simplification that may render the trend of the scaling factor versus this metric un-useful. (2) The range of the mean energies is narrow [1.5–5.3 MeV], and extrapolating the observed energy trend to the full energy range of the XCOM + IAEA data is likely to be inaccurate. Similar to graphite, in figure 3(*b*) for lead, the 0.50% spread of the $\alpha_{\min} - 1$ values for the individual beams is substantially larger than the value of u determined using the graphical method (i.e. 0.04%), and this spread is centred around the $\alpha_{\min}$ value of all the beams combined. Therefore half the spread can be taken to represent the 95% interval (i.e. $u = 0.13\%$) and the more representative 68% and 95% estimates of the lead cross section uncertainty are 0.15% and 0.27%, respectively.

The 95% estimate of cross section uncertainty for lead (0.27%) is very small, and it is different from that for graphite (0.73%). There are two possible reasons for this. (1) Lead is much more efficient than graphite at removing the lower energy component of the incident photon beam that has larger uncertainties/errors. (2) Systematic errors that vary with the atomic number may be unaccounted for in the experiment and/or in the EGSnrc calculations. For instance, the EGSnrc-calculated transmission data are much more sensitive to the choice of the bremsstrahlung angular sampling option for graphite than they are for lead. The effect of different sampling options on transmission values is up to 5% for graphite, but only up to 1% for lead—see figure 6 in Ali *et al* (2012a). Although the most accurate sampling option available is used for all EGSnrc calculations, the accuracy of this option against a ground truth is unknown. Therefore unknown systematic errors in bremsstrahlung angular sampling are likely to have a greater effect on graphite than on lead. Similarly on the experimental side, the challenges in determining the average density and the mass thicknesses were different for graphite versus lead—for graphite, the inhomogeneity of the square bars was the limiting factor, and for lead it was the irregularity of the rod diameters. Also, for a given mass thickness, the linear extent of the graphite bars is much larger than that for lead.

The polyenergetic nature of the incident photon beams has three implications. (1) Lower energy photons are preferentially eliminated by the attenuators, which causes the bulk of the lower transmission signals to be more sensitive to the higher energy part of the spectrum. Therefore the cross section uncertainty estimates that have just been derived are applicable for roughly $\geqslant$1 MeV. (2) Transmission signals are affected by the cross section errors at all the energies in the spectrum, which smears the effect of possible energy-dependent cross section errors and makes the assumption of energy-independent errors less problematic. (3) When indications of possible energy-dependent errors are observed (as is the case for lead), it becomes difficult to interpret them or to include them in the error model.

Overall for the transmission dataset for energies $\geqslant$1 MeV, the energy-independent estimates of photon cross section uncertainty with 68% and 95% confidence are, respectively, 0.6% and 0.7% for graphite, and 0.2% and 0.3% for lead. It is important to note that, despite the subtle details presented above, and regardless of the exact figures for each material, the main point that is clearly supported is that all the estimates are smaller than the current envelope of uncertainty of 1–2%.

3.2. Estimate using the literature dataset

For the dataset of literature cross section measurements, the variation of the reduced χ^2 versus the scaling factor is shown in figure 4. For graphite (183 data points and 182 degrees of freedom), $\alpha_{\min} - 1$ is +0.05% and $\left(\chi_r^2\right)_{\min}$ is 2.2. The value of u from the graphical method is 0.04%, and thus the 68% and 95% estimates of graphite cross section uncertainty are 0.09% and 0.13%, respectively. The corresponding values for lead (105 data points and 104 degrees of freedom) are: $\alpha_{\min} - 1 = -0.50\%$, $\left(\chi_r^2\right)_{\min} = 5.2$, $u = 0.10\%$, and the 68% and 95% estimates of lead cross section uncertainty are 0.60% and 0.70%, respectively. The ratios of the experimental data to the scaled $\alpha_{\min} \times$ (XCOM + IAEA) data are shown in figure 5. Unlike the transmission dataset, $\left(\chi_r^2\right)_{\min}$ values for graphite and lead (2.2 and 5.2, respectively) are much larger than unity, which makes it challenging to interpret the uncertainty estimates above—note that for such a large number of degrees of freedom, the probability of $\left(\chi_r^2\right)_{\min} > 1$ being purely from statistical fluctuations in the experimental data is vanishingly small. The large $\left(\chi_r^2\right)_{\min}$ values could be because the experimental uncertainties are under-estimated and/or because of the presence of systematic energy-dependent errors in the XCOM + IAEA data. Both possibilities are explored here.

For the possibility of under-estimated experimental uncertainty, the experimental data in figure 5 show more scatter relative to what their reported uncertainties suggest, particularly for lead, indicating that some of the experimental uncertainties are under-estimated. To investigate this further, two exercises are performed on the graphite and lead datasets. In the first exercise, any reported experimental uncertainty less than 0.4% is raised to 0.4% before the analysis to determine $\alpha_{\min}$. In the second exercise, experiments with reported uncertainty of 0.4% of less are excluded before the analysis to determine $\alpha_{\min}$. The two exercises are repeated for a cutoff of 0.7% as well. For graphite, the results of the two exercises show that the value of $\alpha_{\min} - 1$ changes by –0.25% to +0.20% around the value obtained with the original dataset (a spread of 0.45%). The corresponding $\left(\chi_r^2\right)_{\min}$ values get to slightly below unity (versus 2.2 for the original dataset). The spread of $\alpha_{\min}$ values that leads to a value of $\left(\chi_r^2\right)_{\min}$ close to unity can be used to determine a more representative estimate of u. Given that the spread is centred around the original $\alpha_{\min}$ value, the 95% interval (i.e. $2u$) can be taken to be half the 0.45% spread (i.e. $u = 0.11\%$). Therefore more representative 68% and 95% estimates of the graphite cross section uncertainty are $|+0.05| + 0.11 = 0.16\%$ and $|+0.05| + 2 \times 0.11 = 0.27\%$, respectively. For lead, the results of the two exercises show that the value of $\alpha_{\min} - 1$ changes from –0.50% by an additional –0.80% in one direction away from unity (a spread of 0.80%). The corresponding lowest $\left(\chi_r^2\right)_{\min}$ is 1.7 (versus 5.2 for the original dataset). Given that the spread is in only one side of the original $\alpha_{\min} - 1$ value, and it is further away from unity, the 95% interval (i.e. $2u$) can be taken as the full 0.80% spread (i.e. $u = 0.40\%$). Therefore more representative 68% and 95% estimates of the graphite cross section uncertainty are $|-0.50| + 0.40 = 0.90\%$ and $|-0.50| + 2 \times 0.40 = 1.30\%$, respectively.

For the possibility of energy-dependent errors in the XCOM + IAEA data, the graphite data in figure 5 indicate negligible energy dependence. The lead data show some energy dependence with a weak positive correlation, suggesting possible deficiencies in the XCOM + IAEA data. Over the energy range in figure 5, it is more likely for lead to have energy-dependent cross section errors compared with graphite because of the larger photoelectric component and because the photonuclear component is relevant at much lower energies (8–20 MeV) than it is for graphite (>17 MeV). In figure 5(*b*), the variation versus energy is ~2.5% . Applying a simple linear model of this variation to the XCOM + IAEA data (not shown) improves $\left(\chi_r^2\right)_{\min}$ from 5.2 to 3.9, but not to unity. A more elaborate energy-dependent model is difficult to establish because the trend with energy is masked by the large scatter in the experimental data. Taking the 2.5% spread as the 95% interval would be overly conservative, given

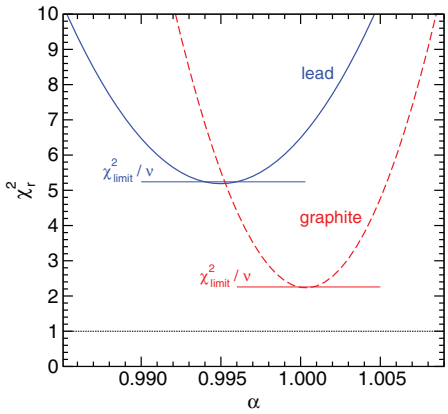

Figure 4. For the literature cross section dataset, variation of the reduced χ^2 when the XCOM + IAEA data for graphite and lead are uniformly scaled by α. χ^2_{limit} / ν is the limit value on χ^2_r at the 68% confidence level for ν degrees of freedom (182 for graphite and 104 for lead).

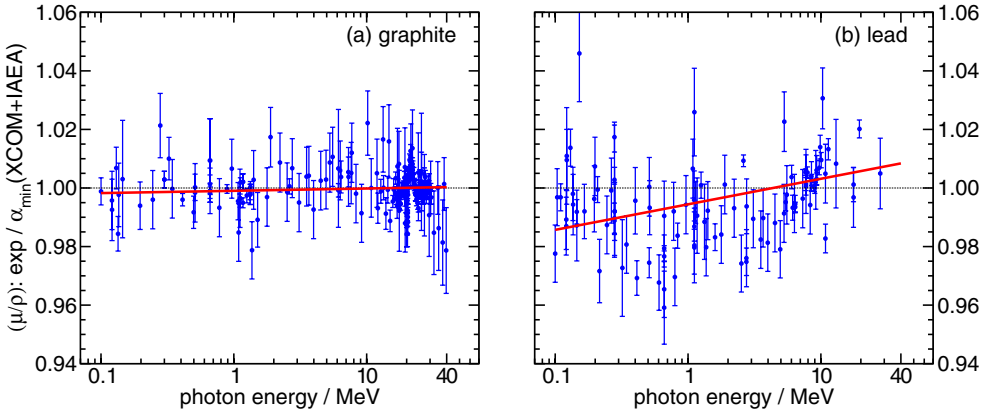

Figure 5. Ratios of the photon cross sections measured in the literature to the scaled cross sections, $\alpha_{min} \times$ (XCOM + IAEA). The XCOM + IAEA data are scaled by +0.05% for graphite (panel (*a*)) and by −0.50% for lead (panel (*b*)). The solid lines are linear fits of the ratios (weighted by the variances on the ratios) versus the logarithm of the photon energy. The uncertainty bars are from the experimental data only.

the large scatter of the experimental data relative to the uncertainty bars, and given the level of agreement in the transmission dataset for lead attenuators.

Overall for the literature cross sections dataset in the energy range 100 keV to 40 MeV, the energy-independent estimates of photon cross section uncertainty with 68% and 95% confidence are, respectively, 0.2% and 0.3% for graphite, and 0.9% and 1.3% for lead.

4. Summary and conclusions

A summary of the results from both datasets is shown in table 1. For a given element, the estimates are different between the two methods, which could be partly because of the energy

Table 1. Estimates of photon cross section uncertainty for graphite and lead, assuming energy-independent errors. ν is the number of degrees of freedom.

	Transmission data			Literature data			Overall	
Element	68%	95%	ν	68%	95%	ν	68%	95%
Graphite	0.6%	0.7%	69	0.2%	0.3%	182	0.5%	0.7%
Lead	0.2%	0.3%	69	0.9%	1.3%	104		

range that each dataset is sensitive to (⩾1 MeV for the transmission dataset versus 100 keV–40 MeV for the literature dataset). The results using the transmission dataset are more *consistent* because $\left(\chi_r^2\right)_{\min}$ is very close to unity without the need for uncertainty scaling. This indicates that the model (i.e. EGSnrc results using $\alpha_{\min}$ × (XCOM + IAEA) data) largely captures the experimental data in accord with the estimated variances (i.e. $s^2_{i,\exp}$ and $s^2_{i,\mathrm{MC}}$ in equation (2)). A single number is desirable as a final result, and it is taken as the average of the four numbers at each confidence level. This is to avoid emphasizing a specific dataset or element (particularly the literature data for lead cross sections where the dataset is clearly *inconsistent*, with a large $\left(\chi_r^2\right)_{\min}$). Therefore, the material-independent energy-independent estimate of photon mass attenuation coefficients is 0.5% (68% confidence) and 0.7% (95% confidence). This estimate applies to the XCOM + IAEA data, or to the XCOM data alone before the threshold of the photonuclear component for a given element. The energy range this estimate applies to is 100 keV to 40 MeV, although it is expected to be less conservative for the lower part of this energy range because of the larger contribution of the photoelectric component with its attendant errors—e.g. the molecular and solid state effects near absorption edges, and the debatable re-normalization factor that was brought back into question by the PTB standards laboratory (Büermann *et al* 2006). The weakest link in the analysis done in this study is the assumption of energy-independent errors. However, it is shown to be a reasonable assumption for the transmission dataset because the photon sources are polyenergetic. For the second dataset, the potential for energy-dependent errors is masked by the scatter in the experimental data.

Depth-dose calculations in a homogeneous water phantom are not very sensitive to small cross section errors, but they are of particular interest in medical physics. Using the final result of this study, the effect of a 0.7% error in water cross sections affects depth-dose curves at 10 cm by ∼0.6% for ^{60}Co, and ∼0.2% for 18 MV (B Muir—personal communication).

The main conclusion of this study is that the uncertainty in photon mass attenuation coefficients in the energy range of interest to external beam radiation therapy is smaller than the currently used envelope of uncertainty of 1–2% . For researchers interested in quantifying the effect of cross section uncertainty on their dosimetric quantities of interest, this study suggests using 0.5% (68% confidence) and 0.7% (95% confidence) as a reasonable estimate.

Acknowledgments

We thank Stephen Seltzer of NIST and Iwan Kawrakow of ViewRay for insightful discussions on the topic, and Bryan Muir (now at NRC) for information on the effect of water cross section errors on depth dose calculations. Elsayed Ali acknowledges funding from a Vanier CGS. Dave Rogers acknowledges funding from the CRC program, NSERC, CFI and OIT.

References

Ali E S M, Mainegra-Hing E and Rogers D W O 2014 Photonuclear attenuation and XCOM cross sections in EGSnrc *Technical Report CLRP* 14–01 (12pp) Carleton University, Ottawa (www.physics.carleton.ca/clrp/photonuclear_xcom)

Ali E S M, McEwen M R and Rogers D W O 2012a Detailed high-accuracy megavoltage transmission measurements: a sensitive experimental benchmark of EGSnrc *Med. Phys.* **39** 5990–6003

Ali E S M, McEwen M R and Rogers D W O 2012b Unfolding linac photon spectra and incident electron energies from experimental transmission data, with direct independent validation *Med. Phys.* **39** 6585–96

Ali E S M and Rogers D W O 2012 An improved physics-based approach for unfolding megavoltage bremsstrahlung spectra using transmission analysis *Med. Phys.* **39** 1663–75

Andreo P, Burns D T and Salvat F 2012 On the uncertainties of photon mass energy-absorption coefficients and their ratios for radiation dosimetry *Phys. Med. Biol.* **57** 2117–36

Bentley R E 2003 *Uncertainty in Measurement: the ISO Guide* 6th edn (Lindfield, NSW: National Measurement Laboratory CSIRO)

Berger M J, Hubbell J H, Seltzer S M, Chang J, Coursey J S, Sukumar R, Zucker D S and Olsen K 2010 XCOM: photon cross section database (version 1.5) *Technical Report* NIST, Gaithersburg, MD (http://physics.nist.gov/xcom)

Büermann L, Grosswendt B, Kramer H M, Selbach H J, Gerlach M, Hoffmann M and Krumrey M 2006 Measurement of the x-ray mass energy-absorption coefficient of air using 3–10 keV synchrotron radiation *Phys. Med. Biol.* **51** 5125–50

Cullen D E, Hubbell J H and Kissel L 1997 EDPL97: the Evaluated Photon Data Library, '97 Version *Report* UCRL-50400, vol 6, rev 5, LLNL, Livermore, CA

Hubbell J H 1982 Photon mass attenuation and energy-absorption coefficients from 1 keV to 20 MeV *Int. J. Appl. Radiat. Isot.* **33** 1269–90

Hubbell J H 1999 Review of photon interaction cross section data in the medical and biological context *Phys. Med. Biol.* **44** R1–22

Hubbell J H and Seltzer S M 1995 Tables of x-ray mass attenuation coefficients and mass energy-absorption coefficients 1 keV to 20 MeV for elements $Z = 1$ to 92 and 48 additional substances of dosimetric interest *Technical Report* NISTIR 5632, NIST, Gaithersburg, MD 20899

IAEA 2000 Handbook of photonuclear data for applications: cross sections and spectra *Technical Report* TECDOC 1178, IAEA (www.nds.iaea.org/photonuclear)

Kawrakow I 2000 Accurate condensed history Monte Carlo simulation of electron transport. I. EGSnrc, the new EGS4 version *Med. Phys.* **27** 485–98

Kawrakow I, Mainegra-Hing E, Rogers D W O, Tessier F and Walters B R B 2011 The EGSnrc Code System: Monte Carlo simulation of electron and photon transport *NRC Technical Report* PIRS-701 v4-2-3-2, National Research Council Canada, Ottawa, Canada (www.nrc-cnrc.gc.ca/eng/solutions/advisory/egsnrc/download_egsnrc.html)

MacPherson M S and Ross C K 1998 A magnetic spectrometer for electron energy calibration *Technical Report* PIRS-0617 pp 59, IRS, NRC, Ottawa, Canada

Muir B R and Rogers D W O 2010 Monte Carlo calculations of k_Q, the beam quality conversion factor *Med. Phys.* **37** 5939–50

Rogers D W O 1975 Analytic and graphical methods for assigning errors to parameters in non-linear least squares fitting *Nucl. Instrum. Methods* **127** 253–60

Ross C K, McEwen M R, McDonald A F, Cojocaru C D and Faddegon B A 2008 Measurement of multiple scattering of 13 and 20 MeV electrons by thin foils *Med. Phys.* **35** 4121–31

Varlamov A, Varlamov V, Rudenko D and Stepanov M 1999 Atlas of giant dipole resonances: parameters and graphs of photonuclear reaction cross sections *Report* INDC(NDS)-394, IAEA Nuclear Data Section, IAEA, Vienna

Walters B R B, Rogers D W O and Shortt K R 1997 Monte Carlo simulation of a cesium irradiator using BEAM *Med. Phys.* **24** 981 (abstract)

Wulff J, Heverhagen J T, Zink K and Kawrakow I 2010 Investigation of systematic uncertainties in Monte Carlo-calculated beam quality correction factors *Phys. Med. Biol.* **55** 4481–93